atmosphere

MDPI

Article

# Climatic and Vegetation Response Patterns over South Africa during the 2010/2011 and 2015/2016 Strong ENSO Phases

**Lerato Shikwambana [1,2,*], Kanya Xongo [1], Morwapula Mashalane [1,2] and Paidamwoyo Mhangara [2]**

[1] Earth Observation Directorate, South African National Space Agency, Pretoria 0001, South Africa
[2] School of Geography, Archaeology and Environmental Studies, University of the Witwatersrand, Johannesburg 2050, South Africa
* Correspondence: lshikwambana@sansa.org.za

**Abstract:** El Niño-Southern Oscillation (ENSO) is a significant climate phenomenon on Earth due to its ability to change the global atmospheric circulation which influences temperature and precipitation across the globe. In this study, we investigate the responses of climatic and vegetation parameters due to two strong ENSO phases, i.e., La Niña (2010/2011) and El Niño (2015/2016) in South Africa. The study aims to understand the influence of strong seasonal ENSO events on climatic and vegetation parameters over South Africa. Remote sensing data from the Global Precipitation Measurement (GPM), Moderate Resolution Imaging Spectroradiometer (MODIS), Modern-Era Retrospective analysis for Research and Applications, version 2 (MERRA-2) and Atmospheric Infrared Sounder (AIRS) was used. The relationship between precipitation, temperature, and Normalized Difference Vegetation Index (NDVI) were studied using Pearson's correlation. Comparison between the La Niña, neutral year, and El Niño periods showed two interesting results: (1) higher precipitation from the south coast to the east coast of South Africa, with some low precipitation in the interior during the La Niña and El Niño periods, and (2) a drop in precipitation by ~46.6% was observed in the southwestern parts of South Africa during the La Niña and El Niño events. The study further showed that wind speed and wind direction were not impacted by strong ENSO events during the MAM, JJA and SON seasons, but the DJF season showed varying wind speeds, especially on the west coast, during both ENSO events. Overall, the Pearson's correlation results clearly showed that the relationship between climatic parameters such as precipitation, temperature, and vegetation parameters such a NDVI is highly correlated while other parameters, such as wind speed and direction, are not. This study has provided new insights into the relationship between temperature, precipitation, and NDVI in South Africa; however, future work will include other climatic and vegetation parameters such as relative humidity and net longwave radiation.

**Keywords:** ENSO; precipitation; temperature; NDVI; correlation

check for updates

**Citation:** Shikwambana, L.; Xongo, K.; Mashalane, M.; Mhangara, P. Climatic and Vegetation Response Patterns over South Africa during the 2010/2011 and 2015/2016 Strong ENSO Phases. *Atmosphere* **2023**, *14*, 416. https://doi.org/10.3390/atmos14020416

Academic Editors: Isaac Nooni, Daniel Fiifi Tawia Hagan, William Amponsah, Nana Agyemang Prempeh and Benjamin Lamptey

Received: 20 January 2023
Revised: 17 February 2023
Accepted: 18 February 2023
Published: 20 February 2023



## 1. Introduction

The El Niño-Southern Oscillation (ENSO) is one of the major climate-related events that account for changes in tropical Pacific Sea surface temperatures (SST). These changes impact tropical weather patterns, but they can also have an impact on a global scale [1,2]. The three distinct ENSO phases are the El Niño, La Niña, and the Neutral phase. During the El Niño phase, southern Africa tends to be drier than normal [3–5]. This dryness has been linked to forced waves displacing the South Indian Convergence Zones [6] or to development of anomalous high pressure over southern Africa and associated reductions in moisture transport [7,8]. The La Niña phase, on the other hand, happens when the SSTs are slightly cooler than normal. The neutral condition occurs when neither El Niño nor La Niña occurs and SSTs in the equatorial Pacific are near average [9].

The changes in precipitation due to ENSO have significant effects on weather and climate, and thus natural vegetation dynamics. However, some of the regional precipitation teleconnections such as the seasonal ones over Southern Africa are still not well

studied. Therefore, the current study provides an analysis of the strong ENSO periods in South Africa to investigate the influence of climatic parameters (precipitation and near surface temperature) on vegetation dynamics using Normalized Difference Vegetation Index (NDVI) as a proxy for the vegetation parameter.

Various studies in southern Africa and globally have conducted ENSO-related studies. For example, Sazib et al. [10] assessed the impact of ENSO on agriculture in Southern and Eastern Africa by exploring the association between ENSO, vegetation condition, and soil moisture. Their results indicate that vegetation conditions are strongly associated with ENSO and show a clear dipole pattern that is reversed between El Niño and La Niña. Ma et al. [11] studied the impact of ENSO on the Australian severe drought from 2018 to early 2020. Erasmi et al. [12] studied the relationship between vegetation greenness and ENSO warm event in Northeastern Brazil. Whan and Zwiers [13] studied the impact of ENSO and the North Atlantic Oscillation on extreme winter precipitation in North America.

The severity of the current climate extremes has enhanced our interest in understanding how ENSO might further affect the Earth's climate in the future. Moreover, the uncertainty in future ENSO SST amplitude changes is significant and is expected to intensify in a warmer world, likely due to the increase in the mean-state atmospheric moisture [14,15]. The main obstacle in assessing future ENSO-related risks is accounting for its large internal variability [16].

Southern Africa receives most of its precipitation in austral summer except for a region in the southwest that experiences austral winter precipitation [17]. During a neutral year, maximum precipitation in the southwest region is recorded in the May to August period (autumn and winter seasons) when the track of the temperate weather systems (i.e., extratropical cyclones, cold fronts, and cutoff lows) is shifted northward [18]. Precipitation in the rest of southern Africa arises from changes in solar insolation and north–south displacement of the Hadley cell [19]. Zonal circulations also play a key role; for example, in the summer, easterly winds draw moisture from the Southwest Indian Ocean and warm Agulhas Current, whereas in winter, westerly winds bring dry air from the South Atlantic Ocean and cool Benguela Current [19]. Wind speed during El Niño/La Niña events is weaker/stronger than normal in the Western Cape region leading to changes in SST [14]. El Niño and La Niña events excite a mid-tropospheric convection dipole between the tropical west and central Pacific, which in turn excites circulation anomalies over southern Africa [8]. Consequently, the anomalous circulations alter the vertical motions and moisture fluxes which then force seasonal southern Africa precipitation anomalies [4,8].

Different circulation patterns can affect vegetation dynamics through their influences on climate extremes. A study by Zhao et al. [20] showed that NDVI had a negative relationship with ENSO in the southern Africa region, indicating that vegetation growth was restrained during El Niño years. Moreover, a study by Georganos et al. [21] concluded that the relationship between precipitation and NDVI varied temporally due to spatial trend differences. In addition, Kalisa et al. [22] further concluded that NDVI correlated higher to precipitation than to temperature.

Satellite, model, and reanalysis datasets have been used extensively by various researchers in the past to measure and correlate climatic and vegetation parameters. For example, Botai et al. [23] used the Tropical Rainfall Measuring Mission (TRMM) satellite to investigate the spatial–temporal variability and trends in precipitation concentration across South Africa for the period of 1998–2015. Their study found that (i) precipitation concentration distribution varies across seasons, and (ii) at an annual timescale, precipitation concentration is highly irregular in most parts of the country. Minnett et al. [24] carried out a study that evaluated sea surface skin temperature ($SST_{skin}$) and atmospheric temperature profiles using the Modern-Era Retrospective Analysis for Research and Applications version 2 (MERRA-2) reanalysis datasets. Jamali et al. [25] used the Moderate Resolution Imaging Spectroradiometer (MODIS) satellite to investigate temporal relationships between vegetation growth, precipitation, and soil moisture for six sites located in sub-Saharan and southern Africa for the period 2005–2009.

To our knowledge, there is a limited number of studies that aim to understand the influence of strong seasonal ENSO events on climatic and vegetation parameters in South Africa. Therefore, this study aims to narrow the knowledge gap. The study aims to understand the influence of strong seasonal ENSO events on climatic and vegetation parameters over South Africa.

## 2. Study Area

South Africa occupies the most southern tip of Africa, stretching latitudinally from 22° S to 35° S and longitudinally from 17° E to 33° E. It has a long coastline stretching more than 3000 km, and its surface area covers ~1,219,602 km$^2$. The country is located within what is considered a 'drought belt' and is the fifth most water-scarce country in sub-Saharan Africa [26]. The topography varies from desert to semi-desert in the drier northwestern region to sub-humid and wet along the country's eastern coast. Approximately half of the country is classified as arid or semi-arid [26]. The average annual rainfall in South Africa is about 464 mm, with the Western Cape getting most of its rainfall in winter (June to August) and the rest of the country receiving summer (December to February) rainfall. Average temperatures in South Africa range from 15 °C to 36 °C in the summer and −2 °C to 26 °C in the winter [26]. Figure 1 shows the 2020 South African National Land-Cover (NLC). The South African NLC is predominantly made up of forested land, shrubland, cultivated land, and barren land. Identifying, delineating, and mapping land cover is important for global monitoring studies, resource management, and planning activities. El Niño in Southern Africa means less rainfall which impacts negatively on agriculture, thus threatening food security. On the other hand, La Niña events mean more rainfall which could lead to flooding in low-lying areas and areas close to riverbanks. Both of these phenomena have been experienced in South Africa thus making the region a perfect candidate for this study.

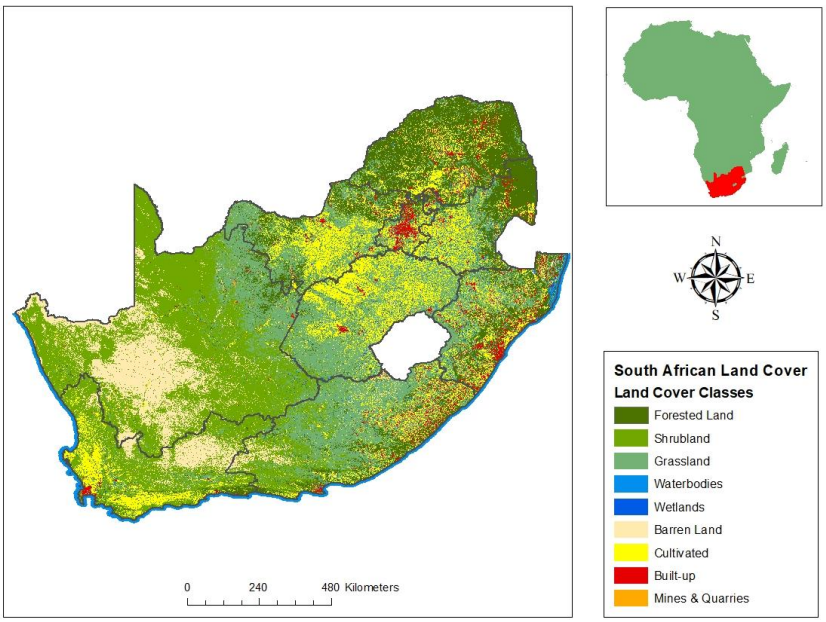


**Figure 1.** Land Cover map of South Africa. The data was retrieved from the South African Department of Forestry, Fisheries and the Environment. (https://egis.environment.gov.za/data_egis/data_download/current, last accessed on 15 November 2022).

## 3. Data and Methods

The data and methods used for this study are summarized in Figure 2, which shows the parameters used and the platforms they are retrieved from.

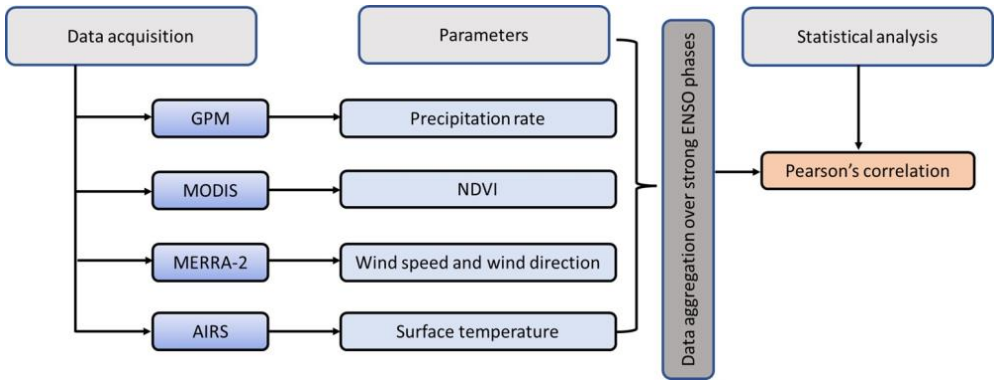


**Figure 2.** Flowchart summarizing the data and methods used in this study.

### *3.1. Data*

#### 3.1.1. Global Precipitation Measurement

The Global Precipitation Measurement (GPM) mission is an international network of satellites that provides the next-generation global observations of rain and snow [27]. The GPM mission is to help advance the understanding of Earth's water and energy cycles, improve forecasting of extreme events that cause natural hazards and disasters, and extend current capabilities in using accurate and timely information of precipitation to directly benefit society [27]. The National Aeronautical and Space Administration (NASA) and the Japanese Aerospace Exploration Agency (JAXA) launched the GPM Core Observatory (GPM-CO) spacecraft in 2014. The GPM-CO was designed to measure rain rates from 0.2–110.0 mm $h^{-1}$, to detect moderate to intense snow events, and to serve as a precipitation physics laboratory [28]. More details about GPM can be found in the references [28–30]. In this study we used the precipitation rate product.

#### 3.1.2. Moderate Resolution Imaging Spectroradiometer

The MODIS instrument is operating on both the Terra and Aqua spacecraft [31]. It has a viewing swath width of 2330 km and views the entire surface of the Earth every 1 to 2 days. Its detectors measure 36 spectral bands between 0.405 and 14.385 µm, and it acquires data at three spatial resolutions—250 m, 500 m, and 1000 m [31]. In this study the MODIS NDVI product is used. The purpose of using NDVI is to improve information analysis about vegetation [28]. NDVI can be used to estimate various vegetation properties such as Leaf Area Index, biomass, plant productivity, fractional vegetation cover, and plant stress [32–36]. More details on the MODIS vegetation index can be found in Huete et al. [37], and details on the specifications and products of MODIS can be found in Justice et al. [38]. In this study we used the NDVI product.

#### 3.1.3. Modern-Era Retrospective analysis for Research and Applications, Version 2

The Modern-Era Retrospective analysis for Research and Applications, version 2 (MERRA-2), is the latest version of global atmospheric reanalysis for the satellite era, produced by NASA Global Modeling and Assimilation Office (GMAO) using the Goddard Earth Observing System Model (GEOS), version 5.12.4 [39]. The dataset covers the period from 1980 to the present with a latency of ~3 weeks after the end of a month [39]. Gridded data are released at a 0.625° longitude × 0.5° latitude resolution on 72 sigma–pressure hybrid layers between the surface and 0.01 hPa [40]. More details on MERRA-2 can be found in the references [41–43]. In this study we used wind speed and wind direction products.

#### 3.1.4. Atmospheric Infrared Sounder

The Atmospheric Infrared Sounder (AIRS) is a hyperspectral infrared instrument aboard NASA's Aqua satellite. It provides measurements of temperature, water vapor, trace gases, and surface and cloud properties through the atmospheric column. AIRS has

2378 infrared channels ranging from 3.7 μm to 15.4 μm [44]. The IR resolution for AIRS is 1 km vertically and 13.5 km horizontally. The VIS/NIR spatial resolution, on the other hand, is ~2.3 km. More details of the instrument are discussed by Chahine et al. [45] and Menzel et al. [46]. In this study, we use the surface temperature product.

A summary of the parameters used in this study is shown in Table 1.

**Table 1.** Dataset used to in this study.

| Input Data Source | Product Used | Time Analysis | Output Data |
|---|---|---|---|
| GPM (0.1°) | Precipitation rate (mm/hr) | 2010-2011<br>2013–2014<br>2015–2016 | • Seasonal spatial distribution map of precipitation |
| MODIS (550 nm) | NDVI | 2010–2011<br>2013–2014<br>2015–2016 | • Seasonal spatial distribution map of NDVI |
| MERRA-2 (550 nm) | Wind speed ($m.s^{-1}$) and wind direction | 2010–2011<br>2013–2014<br>2015–2016 | • Seasonal spatial distribution map of wind speed and direction |
| AIRS (1°) | Temperature (°C) | 2010–2011<br>2013–2014<br>2015–2016 | • Seasonal spatial distribution map of surface temperature |

### *3.2. Methods*

Pearson's Correlation

Pearson's correlation coefficient ($r$) is a measure of the linear association of two variables. The values of the correlation coefficient vary from −1 to +1. Positive values of the correlation coefficient indicate a tendency of one variable to increase or decrease together with another variable [47]. Negative values of the correlation coefficient indicate that the increase of values in one variable is associated with the decrease of values in the other variable and vice versa [47]. Values of the correlation coefficient close to zero indicate a low association between variables, and values close to −1 or +1 indicate a strong linear association between two variables [47].

In this study, Pearson correlation analysis was performed to establish the relationship between the meteorological and vegetation conditions. Each parameter statistic (i.e., regional mean) was extracted using the bounding box shown in the insert map of Figure 1. The specific parameters tested for their relationships are NDVI, precipitation (Precip), and surface temperature (Temp).

The correlation coefficient ($r$) of the random variables $x$ and $y$ is defined by Equation (1) as:

$$r = \frac{\sum(x_i - \overline{x})(y_i - \overline{y})}{\sqrt{\sum(x_i - \overline{x})^2 \sum(y_i - \overline{y})^2}} \quad (1)$$

where, $r$ is the correlation coefficient, variables $x_i$ and $y_i$ represent values for each respective variable $x$ and $y$, respectively, and $\overline{x}$ and $\overline{y}$ are mean values of the $x$ and $y$ variables, respectively. More information on the Pearson correlation test can be found in Benesty et al. [48].

## 4. Results and Discussion

### *4.1. Comparing the Seasonal Spatial Distribution of Precipitation, Temperature, NDVI, and Wind Speed and Direction during the El Niño and La Niña Periods*

The spatial distributions of seasonal precipitation variations during the La Niña, neutral year, and El Niño periods and their differences are shown in Figure 3. The highest precipitation rate in South Africa is observed during the December–January–February (DJF) or summer season (see Figure 3b). Furthermore, comparison between the La Niña, neutral year, and El Niño periods reveals more spatially distributed precipitation in the La Niña period compared to the other seasons (see Figure 3a–c). The DJF precipitation difference shows an increase in precipitation over some parts of South Africa (see Figure 3d). Several

areas in the interior and northeastern parts of South Africa showed an increase in the precipitation rate, whereas another part showed a decrease in the precipitation rate. As mentioned earlier, the La Niña event is generally caused by intensifying trade winds which increase the equatorial upwelling and extends the colder water of the east Pacific westward which then increases precipitation in the region. The drier periods in South Africa, on the other hand, are observed in the June–July–August (JJA) or winter season (see Figure 3j). The southwestern parts of South Africa experience the most precipitation during this season while the rest of the country experiences little to no precipitation. During the JJA season, the northward shift in the South Atlantic high-pressure system carries cold fronts to the west coast. The combination of these cold fronts and the persistent winds over the cold Benguela region introduces precipitation along the west coast of South Africa [49]. Now, comparison between the La Niña, neutral year, and El Niño periods (see Figure 3i–k) shows two interesting results: (1) higher precipitation from the south coast to the east coast of South Africa, with some low precipitation in the interior during the La Niña and El Niño periods, and (2) a drop in precipitation by ~46.6% is observed in the southwestern parts of South Africa during the La Niña and El Niño periods. An unexpected observation was the presence of a region of wetness during the El Niño period. However, this observation is not the first of its kind. During the period of 1997–1998, Lyon and Mason [50] observed moderately dry parts of southern Africa and wetness in others. They concluded that this observation was due to a disruption in the teleconnection by internal atmospheric variability which is not predictable [50].

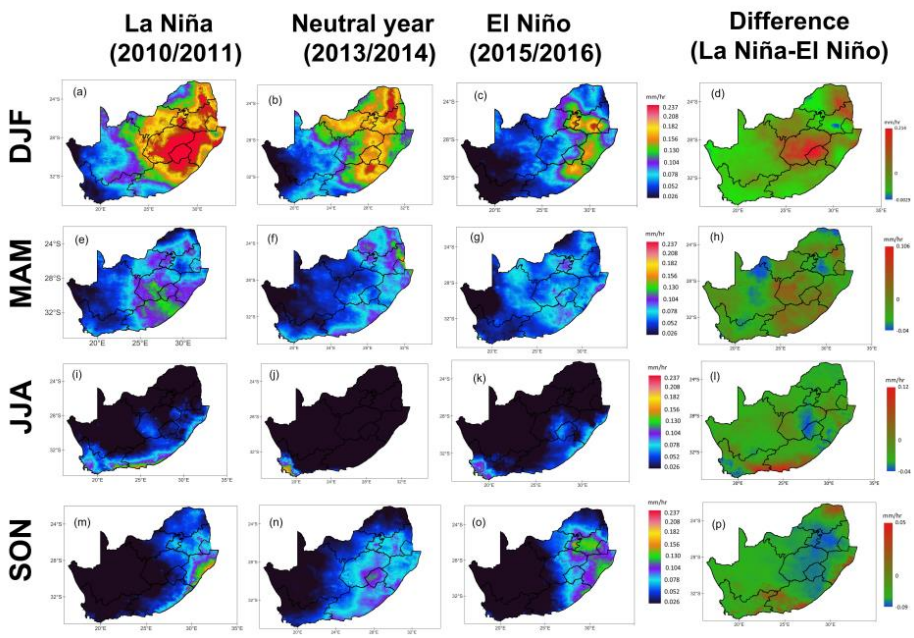


**Figure 3.** Seasonal mean spatial distribution of precipitation during the La Niña (**a**,**e**,**i**,**m**), neutral year (**b**,**f**,**j**,**n**) and El Niño periods (**c**,**g**,**k**,**o**) and the difference between the two extremes (**d**,**h**,**l**,**p**).

A striking difference in the spatial distribution of precipitation in the September–October–November (SON) season is observed in Figure 3m–o. The neutral year shows wetter conditions throughout the country except in the northwest parts of South Africa. On the other hand, both the La Niña and El Niño periods only show the dominance of precipitation in the eastern parts of South Africa. The difference (see Figure 3p) highlights a mixture of increases and decreases in precipitation in certain parts of the country (due to factors such as elevation). An evident decrease in precipitation is observed over the Mpumalanga province (30° E, 26° S) [51]. This area is home to several coal-fired power stations and is the hotspot for most atmospheric emissions (i.e., greenhouse gases (GHG)). Therefore, the reason for the observed decrease in Figure 3p is likely due to increasing

moisture in the atmosphere. As GHG warms the Earth's surface, more water vapor makes its way into the atmosphere. This added moisture boosts the amount of energy needed to heat the atmosphere as SON transitions to DJF, which can shift the timing of precipitation seasons. This means that additional moisture will delay the atmosphere in absorbing energy and producing precipitation.

The spatial distributions of temperature seasonal variations during the La Niña, neutral year, and El Niño periods and their differences are shown in Figure 4. Warm temperatures (greater than 35 °C) are observed during the DJF and SON seasons, while cooler temperatures (less than 25 °C) are observed during the MAM and JJA seasons. The temperature difference in the DJF season (see Figure 4d) shows a decrease in temperature mostly in the interior and northern parts of South Africa during the La Niña period. On the other hand, the coastal areas show a minor increase in temperature during this period which indicates that the southern coastal region is not impacted intensely by La Niña conditions like the inland regions. The minor increase in temperature in the southern coastal region is also observed for other seasons, i.e., March–April–May (MAM), JJA, and SON (see Figure 4h,l,p). During the JJA season (see Figure 4l) a notable unprecedented increase in temperature in the western parts of South Africa is observed indicating high temperatures during the La Niña period. Particularly, an increase in temperature in the area of the red block (see Figure 4l) is significant. It is unclear what the cause of the increase during the JJA season might be. However, the increase is not consistent with the La Niña behavior. The difference in temperature for the SON season (see Figure 4p) also showed some decrease in temperature in interior and northern parts of South Africa. This observation indicates that there are lower temperatures during La Niña. Overall, the results illustrate that La Niña and El Niño affect different parts of South Africa in various ways.

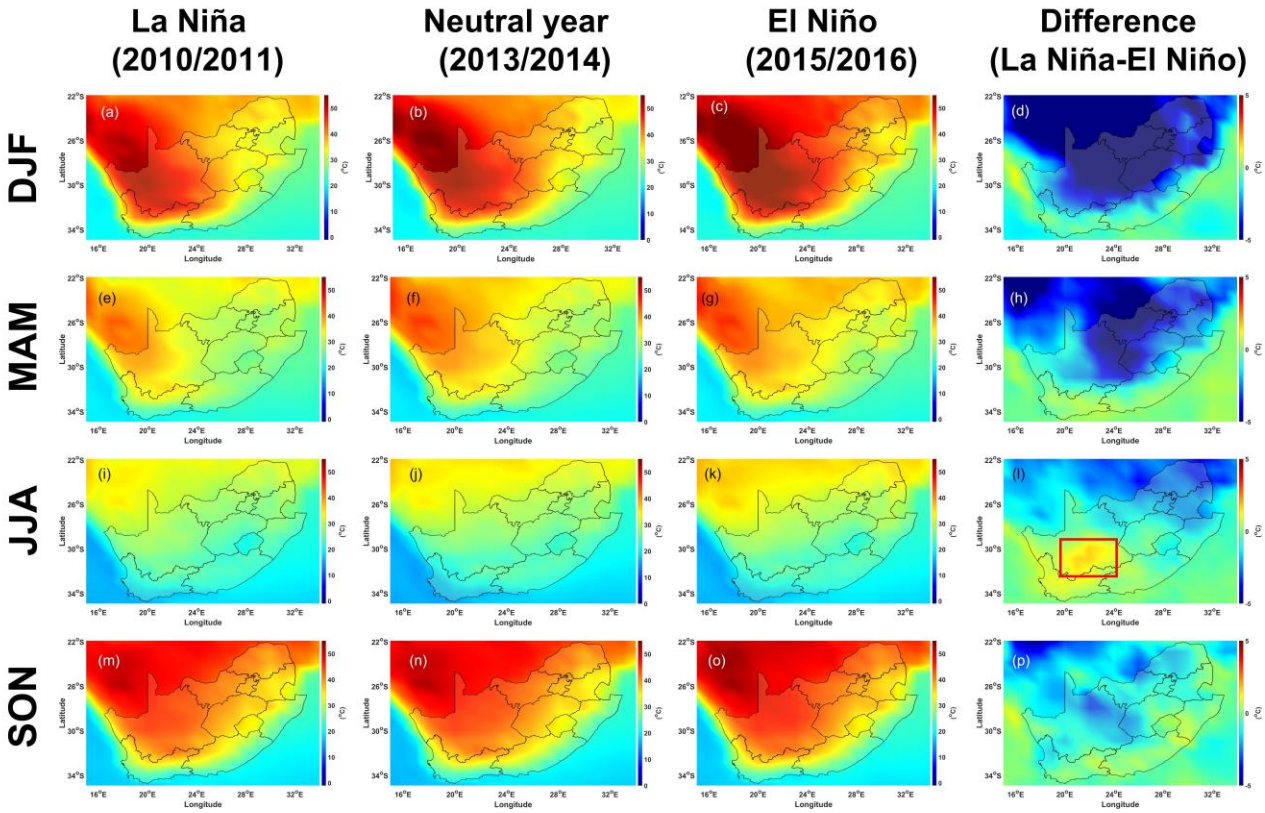


**Figure 4.** Seasonal mean spatial distribution of temperature during La Niña (**a**,**e**,**i**,**m**), neutral year (**b**,**f**,**j**,**n**) and El Niño periods (**c**,**g**,**k**,**o**) and the difference between the two extremes (**d**,**h**,**l**,**p**).

The classification of NDVI in this work follows the works by Simms and Ward [52], Abutaleb et al. [53], and Mondal et al. [54], who grouped NDVI values into three categories

based on quartile distributions. Their interquartile values (middle 50%) were grouped in the class 'intermediate'. The values included in the lowest and highest quartile ranges were assigned to the "low" and "high" NDVI classes, respectively. In this study, NDVI classes are as follows: low (0–0.3), moderate (0.3–0.5) and high (0.5–0.9).

Figure 5 shows the NDVI spatial seasonal patterns during the La Niña, neutral year, and El Niño periods and their differences. One obvious observation in Figure 5 is that low values of NDVI are dominant every season in the northwest parts of South Africa. This is because vast arid plains mostly characterize the landscape. The region receives small amounts of winter rain, and succulent shrubs dominate the landscape [26]. However, the interior and east parts of South Africa are dominated by moderate to high NDVI values. Specifically, the east coast shows high NDVI values every season except for the JJA season where moderate NDVI values are dominant. This is due to less precipitation during the JJA season (see Figure 3). Another interesting observation is the low to moderate NDVI values in the southwestern parts of South Africa during the DJF and MAM seasons. This region receives less precipitation during these periods. On the other hand, high NDVI values are observed during the JJA and SON seasons due to higher precipitation (see Figure 3). The results show that various parts of South Africa exhibit different values of NDVI seasonally, driven by the landcover of that area.

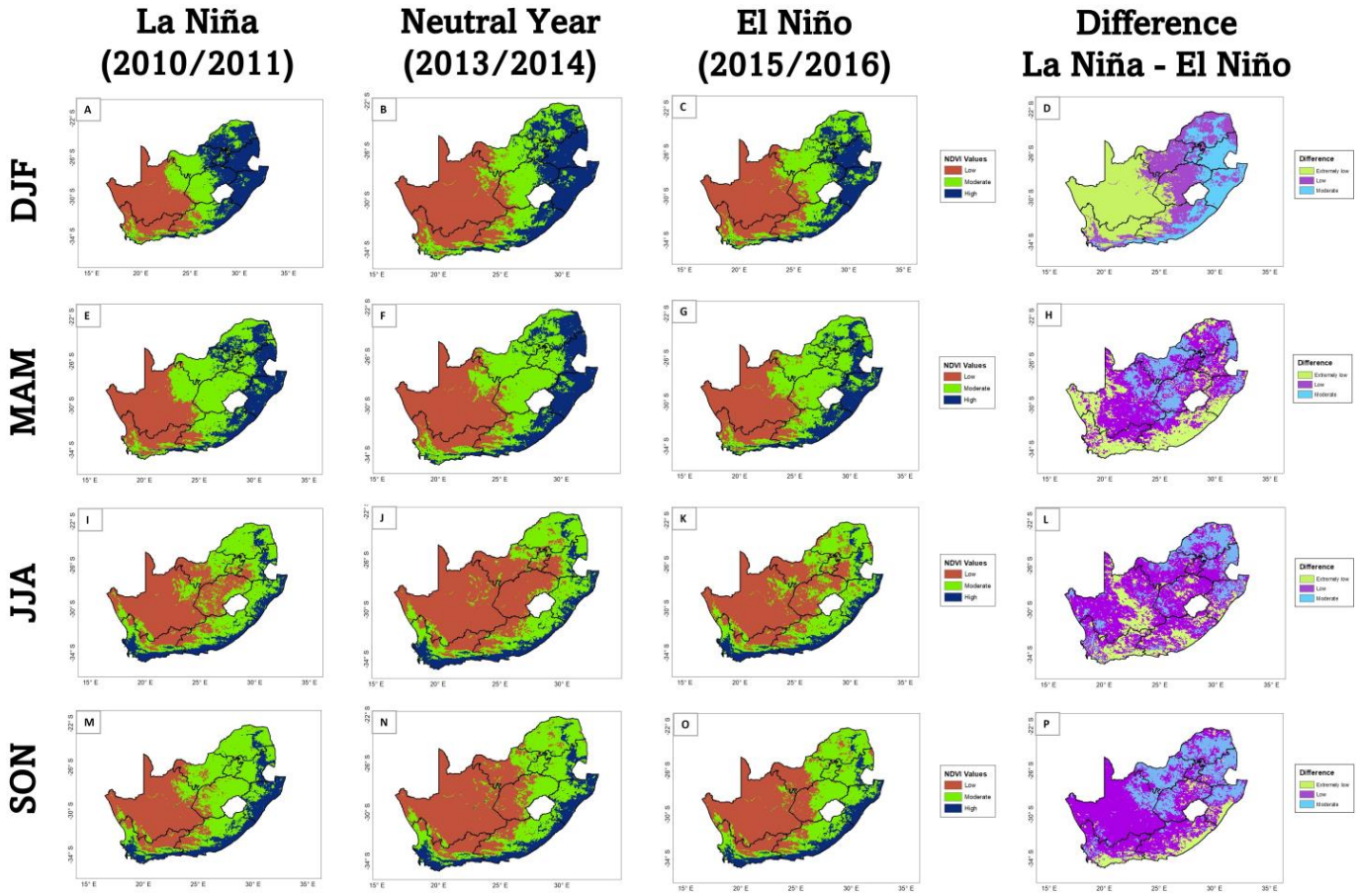


**Figure 5.** Seasonal mean spatial distribution of NDVI during the La Niña (**a**,**e**,**i**,**m**), neutral year (**b**,**f**,**j**,**n**) and El Niño periods (**c**,**g**,**k**,**o**) and the difference between the two extremes (**d**,**h**,**l**,**p**).

The following discussion is limited to the interior and eastern parts of South Africa. During the DJF, the difference (see Figure 5d) shows the dominance of low and moderate NDVI values. This implies an increase in the NDVI values, indicating the presence of greener vegetation. On the contrary, the JJA season (See Figure 5l) shows a mixture of extremely low, low, and moderate NDVI values. The NDVI values are dependent on the

vegetation type in the area. Overall, the results show that high spatial distribution of NDVI values is observed during the La Niña period compared to the El Niño period.

Figure 6 shows the spatial seasonal patterns of wind speed and wind direction during the La Niña, neutral year, and El Niño periods. During the DJF season, the wind speeds and direction for the periods under study are different in some areas. For example, on the west coast, a high wind speed of ~10 m.s$^{-1}$ in a northly direction is observed during the La Niña period (see Figure 6a), whereas slightly lower wind speeds of ~8.3 m.s$^{-1}$ and 9 m.s$^{-1}$ are observed during the neutral year and El Niño period (see Figure 6b,c), respectively. The strong wind-producing mechanism is the extratropical cyclones in the mid latitudes [55]. Furthermore, the wind directions in the northwestern parts of South Africa differ for different periods. The neutral year (see Figure 6b) shows winds travelling in a southerly direction, whereas during the La Niña and El Niño periods, the winds travel in a north-easterly direction. Wind carries moisture along with it; therefore, the direction of the wind will determine where precipitation will occur. This implies that wind direction plays a crucial part in the areas that experience precipitation. Precipitation is essentially directly proportional to the amount of the wind and the moisture content contained in that wind. The wind speed inland is also observed to be low to moderate between 4 m.s$^{-1}$–7 m.s$^{-1}$. The east coast wind speed is ~8.5 m.s$^{-1}$ during the DJF season. The MAM season also shows a wind speed of ~8.5 m.s$^{-1}$ in the east coast of South Africa. The west coast has a slightly slower wind speed of ~9 m.s$^{-1}$, however, there is not much change in the inland wind speed as compared to DJF. During the JJA season (see Figure 6g–i), wind speed in the east coast is higher than the wind speed in the west coast. Even inland, wind speed is slightly higher (maximum wind speed of 8 m.s$^{-1}$) with a large spatial distribution, compared to the observed speed in the DJF and MAM seasons. Berg winds blowing from the plateau are responsible for the JJA winds. Conditions favorable for the occurrence of berg winds are established when the pressure is relatively high over the interior of South Africa with low pressure seaward [56]. The SON season also shows a similar pattern to JJA. Overall, the spatial distributions of wind speed and wind direction are similar for the La Niña and El Niño periods in all seasons.

### *4.2. Comparing Seasonal Correlations between Precipitation, Temperature and NDVI during La Niña, Neutral Year, El Niño Periods*

The results of the statistical relationships between different parameters during the two ENSO phases seasonally are presented in Figure 7. For simplicity of interpretations, the *r* coefficients are grouped into negligible (±0.0 to ±0.3), weak (±0.31 to ±0.5), moderate (±0.51 to ±0.7), high (±0.71 to ±0.9), and very high (±0.91 to ±1.0) negative or positive correlations [57]. The reason for grouping the coefficient in this manner is to improve the understanding of the results. Overall, the results show a moderate to high correlation between NDVI and precipitation (Precip) for all the seasons; however, their values are different for the two ENSO phases. The results show negligible and moderate correlation between NDVI and temperature (Temp) for the DJF, MAM, and SON seasons but not for the JJA season.

During the DJF season, a positive and high/moderate correlation between NDVI and Precip is observed for the La Niña, neutral year, and El Niño periods. The results imply that NDVI tends to increase with increasing precipitation. More precipitation leads to more greenness. Furthermore, a high correlation of 0.82 is observed during the El Niño period, while a moderate correlation of 0.69 is observed during La Niña. This result is surprising as a higher correlation value is expected during the La Niña period. This result implies more precipitation during the El Niño period, resulting in greener vegetation. A negative and weak correlation is observed between Temp and Precip. This result implies that the two parameters are not linked well to each other. Generally, Temp is high during El Niño and Precip is low, and vice versa for La Niña.

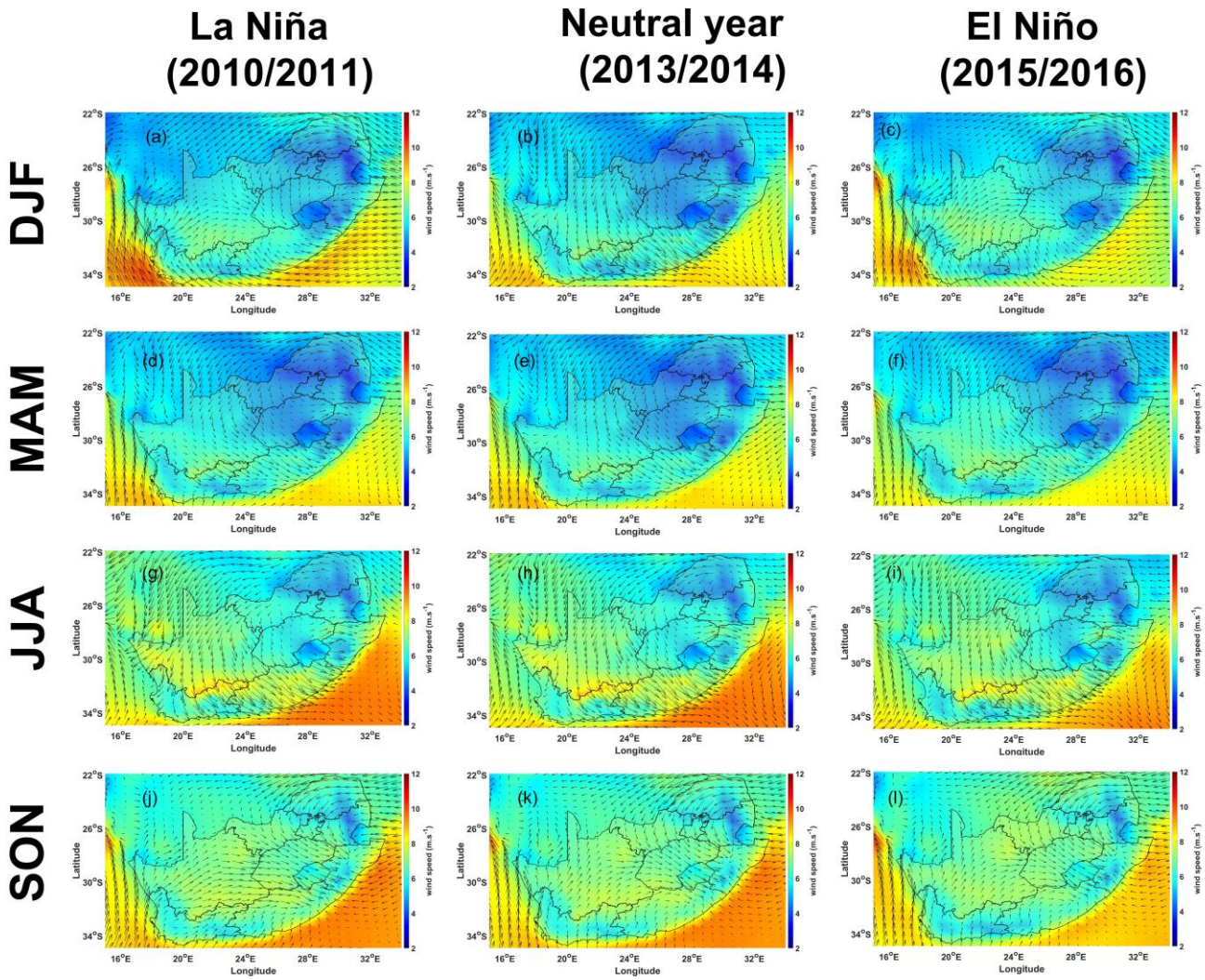


**Figure 6.** Seasonal mean spatial distribution of winds during the La Niña (**a**,**d**,**g**,**j**), neutral (**b**,**e**,**h**,**k**), and El Niño periods (**c**,**f**,**i**,**l**).

During the MAM and SON seasons, a positive and a high/moderate correlation between NDVI and Precip is observed for the La Niña, neutral year, and El Niño periods. However, a high correlation of 0.77 (0.78) is observed during the La Niña period MAM (SON), while a moderate correlation of 0.66 (0.69) is observed during El Niño MAM (SON). The two ENSO phases during MAM and SON have negligible correlation between Temp and Precip; however, the neutral year shows a moderate and negative correlation of −0.61 and −0.67 for MAM and SON seasons, respectively. Other factors not discussed here, such as wind speed, wind direction, and relative humidity, could affect the amount of precipitation, thus affecting the Temp-Precip correlation.

During the JJA season, a positive and a weak/moderate correlation between NDVI and Precip is observed for the La Niña, neutral year, and El Niño periods. The decrease in precipitation during JJA implies a decline in vegetation greenness (low NDVI values). The La Niña period has a slightly higher NDVI value of 0.58 compared to 0.43 for the neutral year and 0.54 for the El Niño period. Of interest is the weak correlation between the Temp and Precip parameters. A higher correlation value of 0.50 is observed during the La Niña period compared to a lower value of 0.33 during the El Niño period. This result implies some degree of linkage between the two parameters during the JJA season. This result suggests that low temperatures in the JJA lead to low precipitation. It is known that as temperatures at the Earth's surface rise, more evaporation occurs, which, in turn, increases

overall precipitation. Therefore, the inverse of this statement is true. Overall, the Pearson's correlation results clearly show that some climatic parameters are highly correlated to vegetation dynamics while others are not.

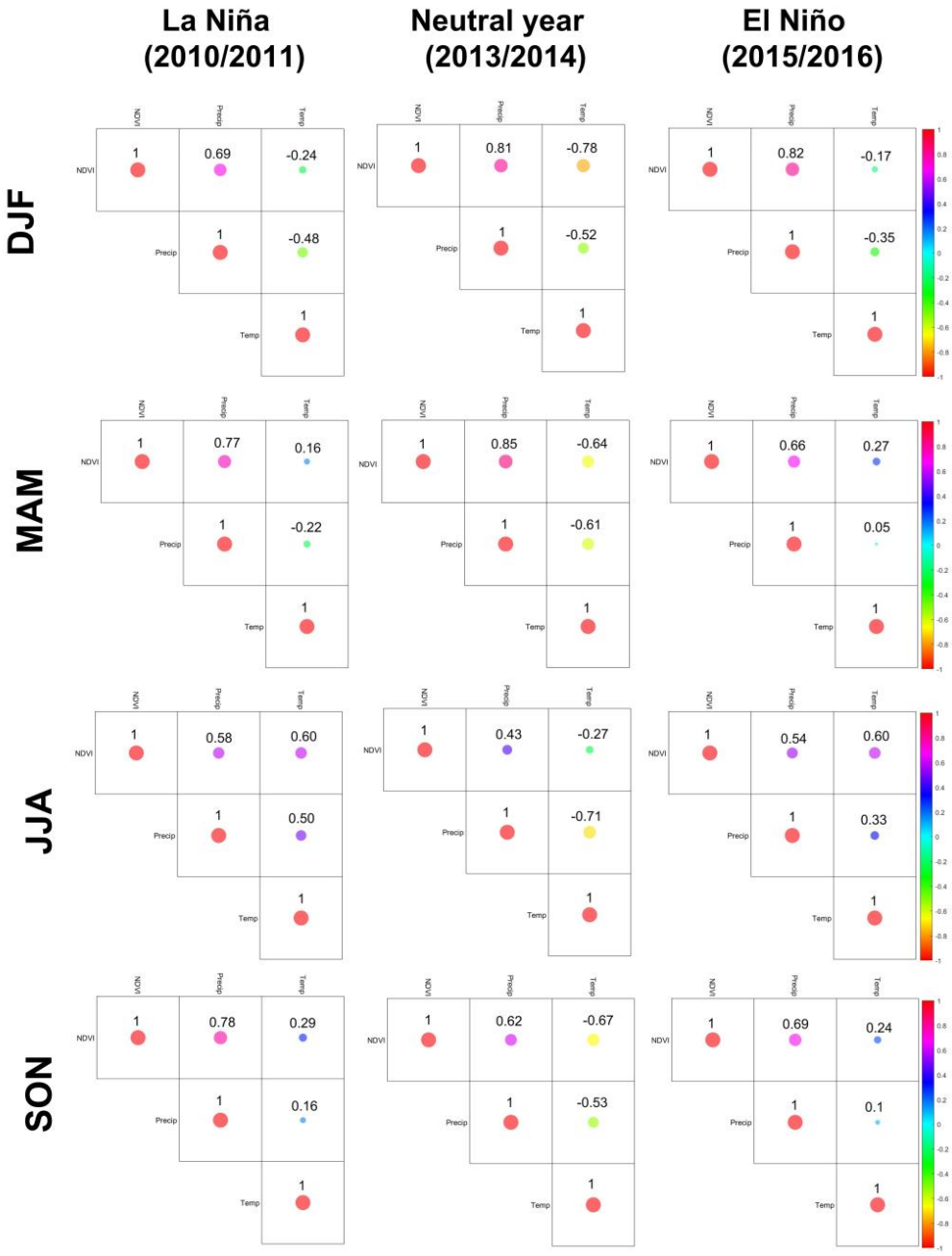


**Figure 7.** The relationship between precipitation (Precip), temperature (Temp), and NDVI during the La Niña, neutral year, and El Niño phases using the Pearson's correlation.

## 5. Conclusions

This study presents a unique take on examining the effects on climatic and vegetation parameters during two strong ENSO events over South Africa during different seasons. South Africa has different climatic regions [58], thus making it complex. It is therefore expected that various regions in the country will react differently to ENSO.

An unexpected result was observed and is shown in Figure 2o; an increased amount of precipitation was seen during the El Niño period rather than the La Niña period in a particular region. It is anticipated that other factors such as atmospheric emissions

contributed to the excessive precipitation. On the other hand, the study shows that wind speed and wind direction are not impacted by strong ENSO events during the MAM, JJA, and SON seasons, while the DJF season showed differences in wind speed for the La Niña and El Niño periods, especially on the west coast. However, seasonal impacts are clearly observed. Overall, the correlation study shows that seasonality plays a vital role in the interactions between the parameters under study. This study has provided new insights into the relationship between these parameters in South Africa. Future work will include (1) correlation with other climatic and vegetation parameters such as relative humidity and net longwave radiation, and (2) forecast analysis of seasonal time series of climatic parameters using machine learning.

**Author Contributions:** Conceptualization, L.S., K.X., M.M. and P.M.; methodology, L.S., K.X. and P.M.; formal analysis, L.S., K.X. and P.M; investigation, L.S., K.X. and M.M.; writing—original draft preparation, L.S.; writing—review and editing, L.S., K.X. and M.M. All authors have read and agreed to the published version of the manuscript.

**Funding:** This research received no external funding. The APC was funded by the South African National Space Agency.

**Institutional Review Board Statement:** Not applicable.

**Informed Consent Statement:** Not applicable.

**Data Availability Statement:** The data that support the findings of this study are openly available in https://giovanni.gsfc.nasa.gov/giovanni/ and https://code.earthengine.google.com/, last accessed on 17 January 2023.

**Acknowledgments:** The author acknowledges the GES-DISC Interactive Online Visualization and Analysis Infrastructure (Giovanni) for providing the MERRA-2, MODIS, and GPM data.

**Conflicts of Interest:** The authors declare no conflict of interest.

## References

1. Hanley, D.E.; Bourassa, M.A.; O'Beiwn, J.J.; Smith, S.R.; Spade, E.R. A Quantitative Evaluation of ENSO Indices. *J. Clim.* **2003**, *16*, 1249–1258. [CrossRef]
2. Mariotti, A. How ENSO impacts precipitation in southwest central Asia. *Geophys. Res. Lett.* **2007**, *34*, L16706. [CrossRef]
3. Mason, S.J.; Jury, M. Climatic variability and change over the southern Africa: A reflection on underlying processes. *Prog. Phys. Geogr.* **1997**, *21*, 23–50. [CrossRef]
4. Reason, C.J.C.; Jagadheesha, D. A model investigation of recent ENSO impacts over Southern Africa. *Meteorol. Atmos. Phys.* **2005**, *89*, 181–205. [CrossRef]
5. Rouault, M.; Richard, Y. Intensity and spatial extent of droughts in southern Africa. *Geophys. Res. Lett.* **2005**, *32*, L15702. [CrossRef]
6. Cook, K.H. A southern Hemisphere wave response to ENSO with implications for southern Africa precipitation. *J. Atmos. Sci.* **2001**, *58*, 2146–2162. [CrossRef]
7. Reason, C.J.C.; Allan, R.J.; Lindesay, J.A.; Ansell, T.J. ENSO and climatic signals across the Indian Ocean basin in the global context: Part I, interannual composite patterns. *Int. J. Climatol.* **2001**, *20*, 1285–1327. [CrossRef]
8. Hoell, A.; Funk, C.; Magadzire, T.; Zinke, J.; Husak, G. El Niño-Southern Oscillation diversity and southern Africa teleconnections during austral summer. *Clim. Dyn.* **2015**, *45*, 1583–1599. [CrossRef]
9. Mulenga, H.; Rouault, M.; Reason, C. Dry summers over northeastern South Africa and associated circulation anomalies. *Clim. Res.* **2005**, *25*, 29–41. [CrossRef]
10. Sazib, N.; Mladenova, L.E.; Bolten, J.D. Assessing the impact of ENSO on agriculture over Africa using earth observation data. *Front. Sustain. Food Syst.* **2020**, *4*, 509914. [CrossRef]
11. Ma, Y.; Sun, J.; Dong, T.; Yu, W.; Dong, W. More profound impact of CP ENSO on Australian spring rainfall in recent decades. *Clim. Dyn.* **2022**, 1–15. [CrossRef]
12. Erasmi, S.; Schucknecht, A.; Barbosa, M.P.; Matschullat, J. Vegetation Greenness in Northeastern Brazil and Its Relation to ENSO Warm Events. *Remote Sens.* **2014**, *6*, 3041–3058. [CrossRef]
13. Whan, K.; Zwiers, F. The impact of ENSO and the NAO on extreme winter precipitation in North America in observations and regional climate models. *Clim. Dyn.* **2017**, *48*, 1401–1411. [CrossRef]
14. Power, S.; Delage, F.; Chung, C.; Kociuba, G.; Keay, K. Robust twenty-first-century projections of El Nino and related precipitation variability. *Nature* **2013**, *502*, 541–545. [CrossRef]
15. Huang, P.; Xie, S.P. Mechanisms of change in ENSO-induced tropical Pacific rainfall variability in a warming climate. *Nat. Geosci.* **2015**, *8*, 922–948. [CrossRef]

16. Fasullo, J.T.; Otto-Bliesner, B.L.; Stevenson, S. ENSO's changing influence on temperature, precipitation, and wildfire in a warming climate. *Geophys. Res. Lett.* **2018**, *45*, 9216–9225. [CrossRef]
17. Philippon, N.; Rouault, M.; Richard, Y.; Favre, A. The influence of ENSO on South Africa winter rainfall. *Int. J. Climatol.* **2012**, *32*, 2333–2347. [CrossRef]
18. Rouault, M.; Richard, Y. Spatial extension and intensity of droughts since 1922 in South Africa. *Water SA* **2003**, *29*, 489–500.
19. Jury, M.R. Climate trends in Southern Africa. *S. Afr. J. Sci.* **2013**, *109*, 1–11. [CrossRef]
20. Zhao, L.; Dai, A.; Dong, B. Changes in global vegetation activity and its driving factors during 1982–2013. *Agric. For. Meteorol.* **2018**, *249*, 198–209. [CrossRef]
21. Georganos, S.; Abdi, A.; Tenenbaum, D.E.; Kalogirou, S. Examining the NDVI-rainfall relationship in the semi-arid Sahel using geographically weighted regression. *J. Arid. Environ.* **2017**, *146*, 64–74. [CrossRef]
22. Kalisa, W.; Igbawua, T.; Henchiri, M.; Ali, S.; Zhang, S.; Bai, Y.; Zhang, J. Assessment of climate impact on vegetation dynamics over East Africa from 1982 to 2015. *Sci. Rep.* **2019**, *9*, 16865. [CrossRef]
23. Botai, C.M.; Botai, J.O.; Adeola, A.M. Spatial distribution of temporal precipitation contrasts in South Africa. *S. Afr. J. Sci.* **2018**, *114*, 70–78. [CrossRef]
24. Luo, B.; Minnett, P.J.; Szczodrak, M.; Nalli, N.R.; Morris, V.R. Accuracy assessment of MERRA-2 and ERA-interim sea surface temperature, air temperature, and humidity profiles over the Atlantic Ocean using AEROSE measurements. *J. Clim.* **2020**, *33*, 6889–6909. [CrossRef]
25. Jamali, S.; Seaquist, J.W.; Ardö, J.; Eklundh, L. Investigating temporal relationships between rainfall, soil moisture and MODIS-derived NDVI and EVI for six sites in Africa. In Proceedings of the 34th International Symposium on Remote Sensing of Environment, Sydney, NSW, Australia, 10–15 April 2011.
26. The World Bank Group. Climate Change Knowledge Portal. Available online: https://climateknowledgeportal.worldbank.org/country/south-africa/climate-data-historical (accessed on 16 November 2022).
27. National Aeronautics and Space Administration. Global Precipitation Measurement. Available online: https://www.nasa.gov/mission_pages/GPM/main/index.html (accessed on 16 November 2022).
28. Skofronick-Jackson, G.; Kirschbaum, D.; Petersen, W.; Huffman, G.; Kidd, C.; Stocker, E.; Kakar, R. The Global Precipitation Measurement (GPM) mission's scientific achievements and societal contributions: Reviewing four years of advanced rain and snow observations. *Q. J. R. Meteorol. Soc.* **2018**, *144*, 27–48. [CrossRef]
29. Skofronick-Jackson, G.; Petersen, W.A.; Berg, W.; Kidd, C.; Stocker, E.F.; Kirschbaum, D.B.; Kakar, R.; Braun, S.A.; Huffman, G.J.; Iguchi, T.; et al. The Global Precipitation Measurement (GPM) mission for science and society. *Bull. Amer. Meteorol. Soc.* **2017**, *98*, 1679–1695. [CrossRef]
30. Skofronick-Jackson, G.M.; Johnson, B.T.; Munchak, S.J. Detection thresholds of falling snow from satellite-borne active and passive sensors. *IEEE Trans. Geosci. Remote Sens.* **2013**, *51*, 4177–4189. [CrossRef]
31. National Aeronautics and Space Administration. MODIS Data. Available online: https://terra.nasa.gov/data/modis-data (accessed on 16 November 2022).
32. Huang, S.; Tang, L.; Hupy, J.P.; Wang, Y.; Shao, G. A commentary review on the use of Normalized Difference Vegetation Index (NDVI) in the era of popular remote sensing. *J. For. Res.* **2021**, *32*, 1–6. [CrossRef]
33. Tian, J.; Wang, L.; Li, X.; Gong, H.; Shi, C.; Zhong, R.; Liu, X. Comparison of UAV and WorldView-2 imagery for mapping leaf area index of mangrove forest. *Int. J. Appl. Earth. Obs. Geoinf.* **2017**, *61*, 22–31. [CrossRef]
34. Zhu, X.; Liu, D. Improving Forest aboveground biomass estimation using seasonal Landsat NDVI time-series. *ISPRS J. Photogramm. Remote Sens.* **2015**, *102*, 222–231. [CrossRef]
35. Vicente-Serrano, S.M.; Camarero, J.J.; Olano, J.M.; Martín-Hernández, N.; Peña-Gallardo, M.; Tomás-Burguera, M.; Gazol, A.; Azorin-Molina, C.; Bhuyan, U.; El Kenawy, A. Diverse relationships between forest growth and the Normalized Difference Vegetation Index at a global scale. *Remote Sens Environ.* **2016**, *187*, 14–29. [CrossRef]
36. Dutrieux, L.P.; Verbesselt, J.; Kooistra, L.; Herold, M. Monitoring Forest cover loss using multiple data streams, a case study of a tropical dry forest in Bolivia. *ISPRS J. Photogramm. Remote Sens.* **2015**, *107*, 112–125. [CrossRef]
37. Huete, A.R.; Didan, K.; Leeuwen, W.J.; Jacobson, A.; Solanos, R.; Laing, T.D. MODIS Vegetation Index (MOD 13). Algorithm theoretical basis document Version 3.1. 1999. Available online: https://vip.arizona.edu/documents/MODIS/MODISVIATBD.pdf (accessed on 16 November 2022).
38. Justice, C.O.; Townshend, J.R.G.; Vermote, E.F.; Masuoka, E.; Wolfe, R.E.; Saleous, N.; Roy, D.P.; Morisette, J.T. An overview of MODIS Land data processing and product status. *Remote Sens. Environ.* **2002**, *83*, 3–15. [CrossRef]
39. National Aeronautics and Space Administration. Atmospheric Composition, Water & Energy Cycles and Climate Variability. Available online: https://disc.gsfc.nasa.gov/datasets/M2I3NPASM5.12.4/summary (accessed on 16 November 2022).
40. Wargan, K.; Labow, G.; Frith, S.; Pawson, S.; Livesey, N.; Partyka, G. Evaluation of the ozone fields in NASA's MERRA-2 reanalysis. *J. Clim.* **2017**, *30*, 2961–2988. [CrossRef]
41. Gelaro, R.; McCarty, W.; Suárez, M.J.; Todling, R.; Molod, A.; Takacs, L.; Randles, C.A.; Darmenov, A.; Bosilovich, M.G.; Reichle, R.; et al. The modern-era retrospective analysis for research and applications, version 2 (MERRA-2). *J. Clim.* **2017**, *30*, 5419–5454. [CrossRef]

42. Buchard, V.; Randles, C.A.; da Silva, A.M.; Darmenov, A.; Colarco, P.R.; Govindaraju, R.; Ferrare, R.; Hair, J.; Beyersdorf, A.J.; Ziemba, L.D.; et al. The MERRA-2 aerosol reanalysis, 1980 onward. Part II: Evaluation and case studies. *J. Clim.* **2017**, *30*, 6851–6872. [CrossRef]
43. Randles, C.A.; da Silva, A.M.; Buchard, V.; Colarco, P.R.; Darmenov, A.; Govindaraju, R.; Smirnov, A.; Holben, B.; Ferrare, R.; Hair, J.; et al. The MERRA-2 aerosol reanalysis, 1980 onward. Part I: System description and data assimilation evaluation. *J. Clim.* **2017**, *30*, 6823–6850. [CrossRef]
44. Pagano, T.S.; Chahine, M.T.; Fetzer, E.J. The Atmospheric Infrared Sounder (AIRS) on the NASA Aqua Spacecraft: A general remote sensing tool for understanding atmospheric structure, dynamics and composition. *Remote Sens. Clouds Atmos. XV* **2010**, *7827*, 162–169.
45. Chahine, M.T.; Pagano, T.; Aumann, H.; Atlas, R.; Barnet, C.; Blaisdell, J.; Chen, L.; Divakarla, M.; Fetzer, E.; Goldberg, M.; et al. AIRS: Improving weather forecasting and providing new data on greenhouse gases. *Bull. Am. Meteorol. Soc.* **2006**, *87*, 911–926. [CrossRef]
46. Menzel, W.P.; Schmit, T.J.; Zhang, P.; Li, J. Satellite-based atmospheric infrared sounder development and applications. *Bull. Am. Meteorol. Soc.* **2018**, *99*, 583–603. [CrossRef]
47. Pearson's Correlation Coefficient. In *Encyclopedia of Public Health*; Kirch, W. (Ed.) Springer: Dordrecht, The Netherlands, 2008; pp. 1090–1091.
48. Benesty, J.; Chen, J.; Huang, Y.; Cohen, I. Pearson Correlation Coefficient. In *Noise Reduction in Speech Processing*; Springer: Berlin/Heidelberg, Germany, 2009; Volume 2, pp. 37–40.
49. Chase, B.M.; Thomas, D.S. Multiphase late quaternary aeolian sediment accumulation in western South Africa: Timing and relationship to paleoclimatic changes inferred from the marine record. *Quat. Int.* **2007**, *166*, 29–41. [CrossRef]
50. Lyon, B.; Mason, S. The 1997/98 summer rainfall season in southern Africa. Part II: Model simulations and coupled model forecasts. *J. Clim.* **2009**, *22*, 3802–3818. [CrossRef]
51. Shikwambana, L.; Sivakumar, V. Investigation of various aerosols over different locations in South Africa using satellite, model simulations and LIDAR. *Meteorol. Appl.* **2019**, *26*, 275–287. [CrossRef]
52. Simms, E.L.; Ward, H. Multisensor NDVI-Based Monitoring of the Tundra-Taiga Interface (Mealy Mountains, Labrador, Canada). *Remote Sens.* **2013**, *5*, 1066–1090. [CrossRef]
53. Abutaleb, K.; Mudede, F.M.; Nkongolo, N. Estimating urban greenness index using remote sensing data: A case study of an affluent vs poor suburbs in the city of Johannesburg. *Egypt. J. Remote Sens.* **2013**, *24*, 343–351. [CrossRef]
54. Mondal, I.; Thakur, S.; De, A.; De, T.K. Application of the METRIC model for mapping evapotranspiration over the Sundarban Biosphere Reserve, India. *Ecol. Indic.* **2022**, *136*, 108553. [CrossRef]
55. Kruger, A.C.; Goliger, A.M.; Retief, J.V.; Sekele, S. Strong wind climatic zones in South Africa. *Wind Struct. Int. J.* **2010**, *13*, 37–55. [CrossRef]
56. van Rooy, M.P. Influence of berg winds on the temperatures along the west coast of South Africa. *Q. J. R. Meteorol. Soc.* **1936**, *62*, 528–537. [CrossRef]
57. Shikwambana, L.; Kganyago, M.; Xulu, S. Analysis of wildfires and associated emissions during the recent strong ENSO phases in Southern Africa using multi-source remotely derived products. *Geocarto Int.* **2022**, 1–17. [CrossRef]
58. Kottek, M.; Grieser, J.; Beck, C.; Rudolf, B.; Rubel, F. World map of the Köppen-Geiger climate classification updated. *Meteorol. Z.* **2006**, *3*, 259–263. [CrossRef]